AIAA JOURNAL
Vol. 38, No. 2, February 2000

Variable N-Factor Method for Transition Prediction in Three-Dimensional Boundary Layers

J. D. Crouch* and L. L. Ng†
The Boeing Company, Seattle, Washington 98124-2207

Linear amplitude methods are presented for estimating the location of transition caused by crossflow instabilities, intended for moderate- to low-turbulence environments. A linear amplitude-based method combines receptivity, linear growth, and an amplitude correlation for predicting transition. Information about the model surface finish (and/or suction distribution) and the freestream disturbance environment is accounted for through the receptivity process. The variable N-factor method is presented as a limiting case, following simplifying assumptions about the receptivity. Transition N factors are presented as a function of the surface roughness. Results show a very good correlation between the variable N-factor method and experimental data.

I. Introduction

BOUNDARY-LAYER transition can play a significant role in estimating airplane aerodynamic performance. Two types of applications that are most sensitive to boundary-layer transition are laminar-flow control applications and separation-sensitive applications (e.g., high-lift design or analysis at off-design conditions). Laminar-flow control seeks to exploit the rather large differences in skin friction between laminar and turbulent boundary layers. High-lift and off-design applications are usually seeking to maximize performance, subject to a large number of constraints, without the adverse effects of large-scale separation.

Motivated by these two types of applications, we present a simplified linear amplitude method for estimating the transition location—trying to balance the desires for improved physical accuracy and for ease of use. Different applications may require different balances between these two desires. Thus, there is a need for a hierarchy of methods with incrementally increasing levels of ease of use and, most likely, incrementally decreasing levels of physical accuracy.

Airplane-performance estimation uses both computational fluid dynamics (CFD) and wind-tunnel testing to predict the airplane characteristics in flight (see, for example, Ref. 1). Wind-tunnel testing is usually done at Reynolds numbers well below the flight condition. If the flow fields at wind tunnel and flight Reynolds numbers are qualitatively similar, the Reynolds-number effects can be accounted for through scaling. This approach may not be viable for transition-sensitive flows because the occurrence of transition provides a qualitative (nonscalable) change in the boundary-layer state. In some cases the low-Reynolds-number boundary layers can be tripped to improve scaling of the results to high Reynolds numbers. This may not be achievable in cases such as high-lift testing because of the large variations in the attachment-line position over the range of angles of attack.[2] For these conditions, some account must be given for the occurrence, or nonoccurrence, of transition.

Transition prediction for aerodynamic flows is usually based on the e^N method.[3,4] An overview of this method is given in Reed et al.[5] In this method the total growth of a family of boundary-layer instability modes is calculated based on linear stability theory. When the total growth exceeds some empirically defined threshold e^N, transition is said to occur. The value of N is based on a collection of wind-tunnel or flight-test data. This method can be very effective when applied to conditions close to the calibration data.

The e^N method considers only the linear growth of disturbances—all other physics (including excitation and nonlinear breakdown) are empirically incorporated into the value of N. If the value of N is calibrated for a particular wind tunnel (with given turbulence and acoustic background levels), there is no a priori reason to expect that value of N to be consistent with observations at other wind tunnels. Likewise, if the value of N is calibrated for a particular model (with given roughness and waviness characteristics), there is no reason to expect that value of N to be consistent with measurements for different models.

A transition-prediction approach based on finite-amplitude disturbances can avoid many of the shortcomings of the e^N method. The finite-amplitude approach involves receptivity, instability growth, and some criteria for transition onset.

Given sufficient information about the freestream environment and the aircraft geometry and surface finish, a nonlinear amplitude-based prediction method can be expected to yield the best estimates of the transition location. To actualize the potential of these methods, detailed information is required about the surface finish and the freestream disturbance environment. These methods also require additional computational effort compared to linear-stability calculations. The level of computational effort depends on the initial spectrum and in some cases can be quite significant. Nonetheless, these methods can be very important to applications such as laminar-flow control when the fidelity of the prediction may be critical.

Other applications, which have less stringent accuracy requirements, may be amenable to simpler linear-amplitude methods. To accommodate these various applications and constraints, a hierarchy of transition-prediction methods is required—from nonlinear amplitude methods, to linear amplitude methods, to variable N-factor methods.

II. Linear Amplitude Methods for Transition Prediction

In many applications the use of nonlinear-interaction methods may not be justified, which can be motivated by the need for reduced computational effort or by the lack of sufficient initial-condition data. Uncertainties in the initial amplitudes may outweigh the improved accuracy of the nonlinear calculation/transition criteria. A linear amplitude-based method provides the potential for significant improvement over the traditional e^N method, without a significant increase in the computational effort.

Mack[6] suggested a linear amplitude-based method as a means of explaining the experimentally observed dependence of transition on the freestream turbulence level. At the time of his study, there were no analytical/numerical models for the various receptivity mechanisms that excite the instabilities. Focusing on turbulence as the source perturbation, Mack proposed an amplitude-based method for Tollmien–Schlichting (TS) wave transition in two-dimensional boundary layers. This method used experimental data to link the

Received 3 September 1998; revision received 10 June 1999; accepted for publication 2 July 1999.

*Associate Technical Fellow, Aeroacoustics and Fluid Mechanics, P.O. Box 3707, MS 67-LF; jeffrey.d.crouch@boeing.com.

†Principal Engineer, Aeroacoustics and Fluid Mechanics; lian.l.ng@boeing.com.

linear instability amplitudes to the freestream turbulence intensity (to the power 2) and to the occurrence of transition. The experimental data showed an N-factor variation proportional to the turbulent intensity to the power 2.4 in reasonable agreement with the linear-amplitude approximation.

Here we exploit more recent developments in the understanding of receptivity to formulate linear-amplitude methods for three-dimensional boundary layers. These methods are aimed at moderately low-disturbance environments with a turbulent intensity $Tu = [(u'^2 + v'^2 + w'^2)/3]^{1/2}$ up to $Tu \approx 0.2\%$. The focus is on crossflow (CF) instabilities where the primary source perturbations are surface roughness and/or suction variations. At moderate turbulence levels the freestream turbulence is also considered as a source perturbation for traveling CF instabilities.

A. Infinite Swept-Wing Flow

We introduce a coordinate system x, y, z, where x is chordwise, z is spanwise, and y is normal to the surface; the corresponding velocities are u, v, w. For the discussion of transition prediction, the unperturbed boundary layer (base flow) is assumed to be spanwise independent, $\partial/\partial z = 0$. Disturbance growth is then limited to the chordwise direction.[7] Linear modes preserve dimensional frequency ω and dimensional spanwise wave number β at different chordwise positions. Focusing on the chordwise velocity component, the disturbance velocity can be written in the form

$$u(x, y, z, t) = \hat{u}(x, y; \beta, \omega) e^{i\beta z - i\omega t} \tag{1}$$

where $\hat{u}$ depends on β and ω parametrically. In general, the instability variation in x is characterized by a chordwise wave number α. This wave number varies with chordwise position and is a function of the frequency and spanwise wave number $\alpha = \alpha(x; \beta, \omega)$.

B. Independent Routes to Transition

The use of a linear-amplitude correlation implies that the various modes of instability evolve independently. Transition is given by the first occurrence of an instability mode (i.e., TS or CF instability) exceeding its linear transition amplitude. Some nonlinear dependence between the modes can be empirically accounted for by allowing the transition amplitude of one mode to be a function of the linear amplitude of another. This is analogous to varying the TS-wave N factor as a function of the CF-instability N factor.

In addition to the distinction between TS and CF instabilities, we consider stationary and traveling CF instabilities as distinct families of modes. This is motivated by the different receptivity mechanisms that generate these instabilities. Stationary CF instabilities are excited directly by steady surface variations; traveling CF instabilities require an unsteady source such as freestream turbulence. The relative importance of stationary and traveling CF modes depends on the freestream turbulence level and their relative growth. These distinctions lead to three different families of modes: TS waves, stationary CF instabilities, and traveling CF instabilities. The focus here is on stationary and traveling CF instabilities.

C. Linear Amplitude Variation

Starting from an initial-amplitude spectrum at x_0, $A(x_0; \beta, \omega)$, the chordwise-varying linear amplitude is given by

$$A(x; \beta, \omega) = A(x_0; \beta, \omega) e^{N(x_0, x; \beta, \omega)} \tag{2}$$

The factor $N(x_0, x; \beta, \omega)$ characterizes the linear amplification of a given mode from x_0 to x, $N(x_0, x; \beta, \omega) = \ln[A(x; \beta, \omega)/A(x_0; \beta, \omega)]$. If x_0 is taken to be the neutral-point location x_I for a given mode, $A(x_I; \beta, \omega)$ is the effective branch-I amplitude, and $N(x_I, x; \beta, \omega)$ is the usual amplification N factor. The linear growth can then be calculated using a typical e^N method.

The N factor may be based on a quasiparallel application of the Orr–Sommerfeld equation or of a reduced lowest-order equation.[8] An alternative approach for calculating the linear growth would be to apply the parabolized stability equations (PSE), which also account for nonparallel effects.[9–11]

For a given family of primary-instability modes (e.g., TS waves, stationary CF instabilities), transition is assumed to occur when any mode within the family reaches a given threshold amplitude A_T. The transition-onset location x_T is determined by the condition

$$\max_{\beta, \omega} A(x_T; \beta, \omega) = A_T \tag{3}$$

The value of A_T is determined empirically and will show some dependence on the environmental conditions. Each family of modes has its own value of A_T, which we write as A_{SCF} and A_{TCF} for stationary CF instabilities and traveling CF instabilities, respectively. Note that A_T is an effective linear amplitude and thus may not correspond to the measured transition amplitude of an experiment.

The combination of Eqs. (2) and (3) provides a link between transition and the initial disturbance levels. This requires a receptivity calculation in addition to the linear-stability calculation. The transition prediction is described by three (somewhat distinct) elements: the receptivity amplitudes $A(x_0; \beta, \omega)$, the instability growth $N(x_0, x; \beta, \omega)$, and the transition-amplitude criteria A_T. The values of A_T (for the different instabilities) are based on empirical criteria, but the initial amplitudes and the linear growth can, in principle, be determined theoretically.

III. Variable N-Factor Method

The idea of variable N factors is not new—in fact, the value of N often varies from one application to another. This is not surprising because all of the receptivity and nonlinear physics are incorporated into the N factor. Each new application requires a new calibration for N. To expand the applicability of the e^N method and reduce the need for calibration, a systematic (a priori) variation of the N factor is required.

Mack[6] provides one of the earliest attempts to systematically model the variation of N associated with TS-wave transition. Using flat-plate wind-tunnel data, Mack deduced a variation of N with the freestream turbulence intensity Tu:

$$N = -8.43 - 2.4 \ln(Tu) \tag{4}$$

A value of $N = 9$ is obtained for a turbulence intensity of 0.07%. This correlation appears most useful at higher turbulence levels where the turbulence can be a dominant source of instability excitation. At low turbulence levels (below $Tu \approx 0.2\%$), acoustic fluctuations play an equal or greater role in influencing TS-wave transition.

Here we focus on CF instabilities in low-to-moderate disturbance environments. Crouch[12] and Radeztsky et al.[13] have suggested that the stationary-CF N factor may be linked to surface roughness. The variable N-factor method is considered as a limiting case of the linear-amplitude method presented in Sec. II. The value of N is varied in accordance with the receptivity theory, and the effective linear amplitude at transition is assumed to be a constant for a given type of instability. Thus the range of applicability of the N-factor method is extended by including the receptivity in the value of N at transition.

A. Receptivity Approximations

An amplitude-based method requires the ability to determine the initial amplitudes for the relevant instability modes. Reviews of the basic receptivity physics and summaries of the different receptivity mechanisms are given in the papers of Goldstein and Hultgren,[14] Saric et al.,[15] Wlezien,[16] Choudhari and Streett,[17] and Crouch.[18] Here, the dominant surface variation is considered to be nonlocalized with a nearly uniform spectrum over the range of unstable wave numbers. The details of the spectrum can be neglected, and the surface roughness (or suction) variation can be characterized by the nondimensional rms variation δ. The freestream turbulence is characterized by the turbulence intensity Tu. Stationary CF instabilities are excited by surface roughness or by variations in the surface suction velocity. Assuming that the nonlocalized-receptivity coefficient varies weakly over the band of relevant modes, we can write the effective branch-I amplitude for stationary CF instabilities as

$$A(x_I; \beta, 0) = \delta \bar{C}_{\mathrm{SCF}} \tag{5}$$

The receptivity coefficient $\bar{C}_{\mathrm{SCF}}$ depends on the details of the receptivity process, but is considered to be independent of β.

The excitation of traveling CF instabilities involves unsteady freestream disturbances, possibly in combination with surface roughness (or suction variations). Receptivity analyses show the acoustic receptivity for traveling CF instabilities results in initial amplitudes much smaller than the stationary-CF amplitudes generated by the same surface roughness (or suction). Estimates based on an acoustic amplitude of approximately 0.01% of the edge velocity show an initial stationary-mode amplitude 100 times larger than a corresponding traveling mode.[12] This suggests a strong bias toward stationary CF modes in low-disturbance environments.[12,19] A bias toward stationary modes was observed in the experiments of Muller and Bippes[20] and Takagi et al.[21]; however, as the level of freestream disturbances is increased, traveling CF instabilities become more important.[22] Likewise, Takagi and Itoh[23] have shown that a reduction in surface roughness, with fixed freestream disturbance levels, increases the importance of traveling CF instabilities.

The combination of the experiments and the analysis suggests that the excitation of the traveling CF modes is more the result of turbulence than of acoustic fluctuations. Neglecting the details of the surface-variation and turbulence spectra and assuming a linear dependence on δ, the branch-I traveling-CF amplitude is written as

$$A(x_I; \beta, \omega) = \delta \bar{C}_{\mathrm{TCF}} \tag{6}$$

The receptivity coefficient $\bar{C}_{\mathrm{TCF}}$ depends on the turbulence intensity Tu, but is considered to be independent of β and ω. Equation (6) implies that the receptivity results from a coupling between the turbulence and the surface variation. A more explicit treatment of the turbulence level will require a better understanding of the detailed mechanism by which the traveling modes are excited.

The value of δ is based on local scaling in the neighborhood of the neutral points, $x = x_I$. For surface roughness or waviness δ is an rms height nondimensionalized by the local boundary-layer displacement thickness δ^* based on the streamwise velocity profile. For surface suction δ is an rms velocity nondimensionalized by the local edge velocity. Thus the variable N factor accounts for some of the unit-Reynolds-number effects through the local scaling. A change in the unit Reynolds number will change the reference quantities at a given chord position and, in some cases, also the chord position of the neutral points. Further details about the receptivity, including some receptivity coefficients, are given in Ref. 18.

B. Stationary CF Transition

For low-disturbance environments, experiments show a significant bias toward stationary modes of CF instability. The experiments of Takagi et al.[21] show no significant traveling CF instability with a turbulence intensity of $Tu \approx 0.02\%$. At higher turbulence levels traveling CF modes become important and eventually the dominant mode of CF instability.[22]

Focusing on low-disturbance environments the transition can be expected to correlate most strongly with the stationary CF-instability amplitude. Combining Eq. (5) with Eqs. (2) and (3), the stationary CF amplitudes at transition satisfy the condition

$$\max_{\beta} \left[\delta \bar{C}_{\mathrm{SCF}} e^{N(x_I, x_T; \beta, 0)} \right] = A_{\mathrm{SCF}} \tag{7}$$

Introducing N_{SCF} as the stationary CF-instability N factor at transition, Eq. (7) becomes

$$N_{\mathrm{SCF}} \equiv \max_{\beta} [N(x_I, x_T; \beta, 0)] = \ln \left(\frac{A_{\mathrm{SCF}}}{\delta \bar{C}_{\mathrm{SCF}}} \right) \tag{8}$$

Expanding the right-hand side of Eq. (8) and introducing $N_{\mathrm{SCF}0} = \ln(A_{\mathrm{SCF}}/\bar{C}_{\mathrm{SCF}})$ gives

$$N_{\mathrm{SCF}} = N_{\mathrm{SCF}0} - \ln(\delta) \tag{9}$$

The quantity $N_{\mathrm{SCF}0} = \ln(A_{\mathrm{SCF}}/\bar{C}_{\mathrm{SCF}})$ is a reference N factor that depends on the particular nondimensionalization of δ. The form of Eq. (9) is in agreement with the analysis of Crouch[12] and the observations and suggestions of Radeztsky et al.[13]

For given levels of roughness (or suction variation) δ, the stationary CF instability N factor N_{SCF} can be experimentally determined. The value of $N_{\mathrm{SCF}0}$ can then be backed out of Eq. (9). Alternatively, $\bar{C}_{\mathrm{SCF}}$ can be calculated from receptivity theory and combined with A_{SCF} to calculate $N_{\mathrm{SCF}0}$. With $N_{\mathrm{SCF}0}$ known, the N factor for any value of the roughness (or suction) is given by Eq. (9).

C. Traveling CF Transition

As discussed in Sec. III.A., traveling CF instabilities play a dominant role in transition for higher freestream disturbance levels. For these conditions the transition location is linked to the traveling CF amplitude. Combining Eq. (6) with Eqs. (2) and (3), the traveling CF amplitudes at transition satisfy the condition

$$\max_{\beta, \omega} \left[\delta \bar{C}_{\mathrm{TCF}} e^{N(x_I, x_T; \beta, \omega)} \right] = A_{\mathrm{TCF}} \tag{10}$$

Introducing N_{TCF} as the traveling CF-instability N factor at transition, Eq. (10) becomes

$$N_{\mathrm{TCF}} \equiv \max_{\beta, \omega} [N(x_I, x_T; \beta, \omega)] = \ln \left(\frac{A_{\mathrm{TCF}}}{\delta \bar{C}_{\mathrm{TCF}}} \right) \tag{11}$$

Expanding the right-hand side of Eq. (11) and introducing $N_{\mathrm{TCF}0} = \ln(A_{\mathrm{TCF}}/\bar{C}_{\mathrm{TCF}})$ gives

$$N_{\mathrm{TCF}} = N_{\mathrm{TCF}0} - \ln(\delta) \tag{12}$$

In this case the reference N factor $N_{\mathrm{TCF}0}$ depends on the turbulence intensity Tu. The value of $N_{\mathrm{TCF}0}$ is determined from an experimental N_{TCF} for a given level of roughness (or suction variation) δ and a given turbulence intensity Tu using Eq. (12).

IV. Variable N-Factor Results

Figure 1 shows the variation of the stationary CF instability N factor for different levels of surface roughness. The symbols show the experimental data of Radeztsky et al.[13] based on quasiparallel N factors. Radeztsky et al.[13] have noted that the CF-instability amplitude ratios appeared to vary as the inverse of the roughness height and that this provided a potential quantitative link between N factors and roughness. The data points are for the highest Reynolds numbers considered for each surface roughness in order to avoid cases where

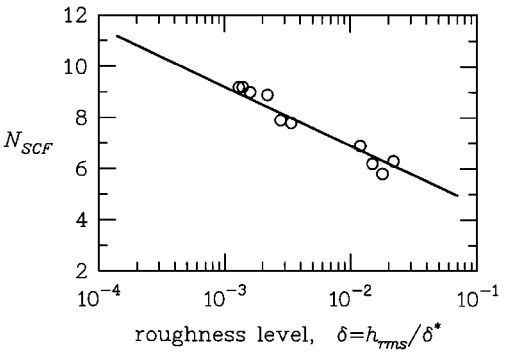

Fig. 1 Stationary CF-instability N-factor variation with surface roughness level ($N_{\mathrm{SCF}0} = 2.3$). Quasiparallel calculations based on experiments of Radeztsky et al.[13]; $Tu = 0.02\%$.

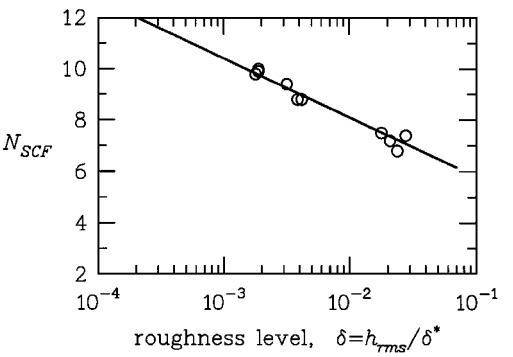

Fig. 2 Stationary CF-instability N-factor variation with surface roughness level ($N_{\mathrm{SCF}0} = 3.5$). Nonparallel calculations based on experiments of Radeztsky et al.[13]; $Tu = 0.02\%$.

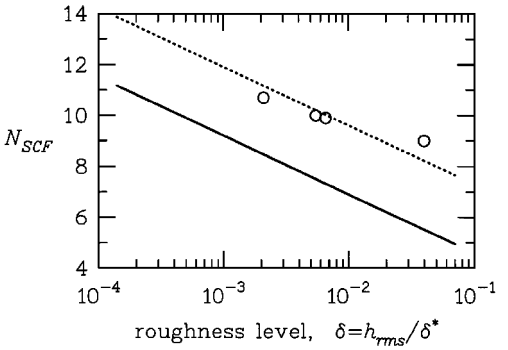

Fig. 3 Stationary CF-instability *N*-factor variation with surface roughness level ($N_{SCF0} = 5.0$). Quasiparallel calculations based on experiments of Deyhle and Bippes[22]; $Tu = 0.15\%$. The solid line is from Fig. 1 ($N_{SCF0} = 2.3$).

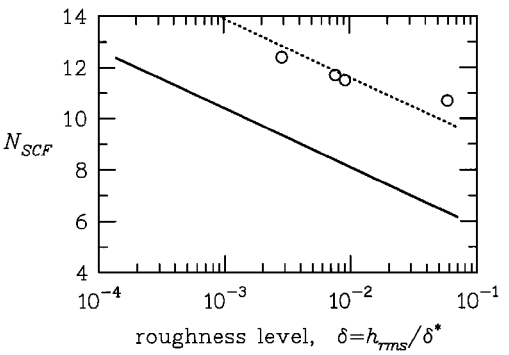

Fig. 4 Stationary CF-instability *N*-factor variation with surface roughness level ($N_{SCF0} = 7.0$). Nonparallel calculations based on experiments of Deyhle and Bippes[22]; $Tu = 0.15\%$. The solid line is from Fig. 2 ($N_{SCF0} = 3.5$).

the transition occurred close to the pressure minimum. Additional details for the calculations are given in the Appendix. The freestream turbulence intensity is $Tu = 0.02\%$ over the range 2 Hz–1 KHz; detailed measurements show vortical disturbances to be dominant over acoustic disturbances in this frequency range. Transition locations are based on naphthalene flow visualization and correspond to the location of the rapid rise in u'. The roughness height δ is an integral rms level filtered 20–1500 μm. These length scales are below the wavelengths for the instabilities, but the rms values should provide a representative measure of the roughness. The roughness height is nondimensionalized by the streamwise-profile displacement thickness δ^* at the neutral point location for the critical mode (i.e., the mode with the maximum value of N at x_T). The solid line is obtained from Eq. (9) with $N_{SCF0} = 2.3$, determined from the experimental fit. This comparison shows a good correlation between the variable N factor surface roughness.

Figure 2 shows the variation of the stationary CF N factor for the experimental data of Radeztsky et al.,[13] now based on nonparallel N factors calculated using the PSE code ECLIPSE[24] (see the Appendix for details). When the nonparallel and curvature effects are included, the reference N factor is increased to $N_{SCF0} = 3.5$. The shift of the data points toward higher roughness values (compared to Fig. 1) is caused by the upstream movement of the nonparallel neutral points. The degree of correlation is slightly improved by the inclusion of the nonparallel and surface-curvature effects. This relatively small change can be expected because the nonparallel and surface-curvature effects occur primarily in a narrow zone near the leading edge and the net change in growth rate is about the same for all of the cases considered. When considering a different model, the N factors based on nonparallel and surface-curvature effects may provide a better correlation.

Figure 3 shows the variation of the stationary CF N factor for the experimental data of Deyhle and Bippes[22] based on quasiparallel analysis as described in the Appendix. The rms roughness levels were estimated from the measured peak-to-peak values by dividing by $2\sqrt{2}$. The freestream turbulence intensity for this case is $Tu = 0.15\%$ over the range 2 Hz–2 KHz; measurements show vortical disturbances to be dominant over this range of frequencies. These data do not collapse as well as the results of Fig. 1. In addition, the reference N factor (used for the dashed line) is $N_{SCF0} = 5.0$ compared to a value of 2.3 from Fig. 1. Nonparallel calculations are presented in Fig. 4. Inclusion of the nonparallel effects does not improve the level of collapse or the degree of comparison with the N_{SCF0} value from the Radeztsky et al. data.[13] The differences in the correlations for the two experiments may be caused, in part, by differences in the measures and filters used for the rms values.

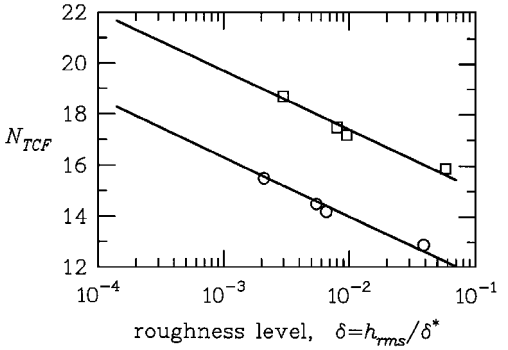

Fig. 5 Traveling CF-instability *N*-factor variation with surface roughness level. Quasiparallel (○, $N_{TCF0} = 9.4$) and nonparallel (□, $N_{TCF0} = 12.8$) calculations based on experiments of Deyhle and Bippes[22]; $Tu = 0.15\%$.

These differences may also be the result of differences in the turbulent intensity. This would suggest that larger linear transition amplitudes are achieved in higher-turbulence flows. In fact, at $Tu = 0.15\%$ traveling CF instabilities may be more strongly linked to the occurrence of transition. Experiments of Muller and Bippes[20] show stationary CF instability to have larger amplitudes than traveling CF instability at $Tu = 0.08\%$; however, at $Tu = 0.15\%$ the traveling CF is initially larger. The experiments of Deyhle and Bippes[22] show an increasing role of traveling CF modes as the turbulence intensity is increased. When the turbulence level exceeds $Tu \approx 0.2\%$, the traveling modes become dominant.

Figure 5 shows the variation of the traveling CF N factor for the experimental data of Deyhle and Bippes[22]; both quasiparallel and nonparallel results are given (see the Appendix for additional details). The data compare very well with the traveling CF variable N factor using a reference value of $N_{TCF0} = 9.4$ or 12.8 for quasiparallel or nonparallel calculations, respectively. The results of Fig. 5 were based on the traveling-CF receptivity described by Eq. (6). Note, however, that similar results could be obtained even if the traveling CF receptivity were independent of the roughness δ; this would occur if the traveling-CF transition amplitude A_{TCF} depended linearly on the stationary-CF amplitude (which depends on δ).

To the degree that the linear approximation is justified, the results of Figs. 3–5 suggest that traveling CF instabilities are dominant for transition at turbulence levels $Tu \approx 0.15\%$. This is further supported by the results of Masad and Abdelnaser.[25] Their analysis suggests that traveling CF instability is responsible for transition in the swept-cylinder experiments of Poll,[26] which were conducted at a moderately low turbulence level, $Tu < 0.16\%$. The stronger amplification of the traveling CF instabilities can offset a receptivity bias toward stationary modes.

The transition data of Poll[26] were reasonably well correlated with a nonparallel traveling CF-instability N factor of 15 (Ref. 25). Calculations of Malik and Balakumar[27] show very little N-factor change resulting from the combined nonparallel and surface-curvature effects for the experimental configuration of Poll.[26] From Fig. 5 an N factor of 15 would correspond to an rms roughness level of approximately $0.004\delta^*$ based on a quasiparallel results and $0.11\delta^*$ based on nonparallel results. For an estimated neutral-point displacement thickness $\delta^* \approx 0.1$ mm the corresponding rms surface roughness would be $h_{rms} \approx 0.4$ or 10 μm for quasiparallel or nonparallel correlations, respectively. The actual roughness level was not measured in the experiment.

Based on the experimental results and correlations, the estimated transition is linked to the stationary CF instabilities for very low turbulence intensities $Tu \approx 0.02\%$ and to the traveling CF instabilities for moderate turbulence intensities $Tu \approx 0.15\%$. Further refinements will require additional experimental data at different turbulence levels.

V. Conclusions

The variable N-factor method provides an improvement over the usual N-factor approach without additional computation. This method could be very useful for applications in which the disturbance environment and the model finish are only known by some nominal measures and/or a minimum computational effort is required.

The variable N factor assumes a correlation between the transition onset and the linear amplitude of the relevant instabilities. Initial amplitudes for the instabilities are linked to the nonlocalized receptivity through a simplified model. The method requires a measure of the surface roughness variation, or surface suction variation, in the neighborhood of the instability neutral points (where nonlocalized receptivity occurs). Significant localized receptivity sources, such as a single row of roughness elements, are not accounted for in the N-factor variation.

Results show good agreement between the variable N-factor method and experiments for CF-instability transition. For low-turbulence environments $Tu \approx 0.02\%$, the transition onset is linked to stationary CF instabilities. Values for the stationary CF-instability N factor are presented based on the experiments of Radeztsky et al.[13] For moderate-turbulence environments with $Tu \approx 0.15\%$, the transition onset is linked to traveling CF instabilities. Values for the traveling CF-instability N factor are based on the experiments of Deyhle and Bippes.[22] Variable N factors are presented as a function of the normalized rms surface-roughness variation for both stationary and traveling CF instabilities.

Appendix: N-Factor Calculations

Details for the calculations of Figs. 1–5 are given in Tables A1–A5, respectively. The variables presented include Reynolds number $R_C = Q_\infty C/\nu$, streamwise displacement thickness at the critical-mode neutral point δ^*, nondimensional roughness height $\delta = h_{\rm rms}/\delta^*$, transition N factor $N_{\rm SCF}$ or $N_{\rm TCF}$, and the critical-mode spanwise wavelength λ_z. The wing chord C is measured in the direction of the freestream velocity Q_∞. The nonparallel N factors are based on the chordwise u-profile maximum.

The calculations for the experiment of Radeztsky et al.[13] are based on their Fig. 2 and on the computational Cp given in Haynes and Reed.[28] Earlier studies have shown good agreement between theory and experiment for instability growth[28] and for localized receptivity[29] based on these flow conditions.

The calculations for the experiment of Deyhle and Bippes[22] are based on the 1 MK Cp given in their Fig. 3. The effective freestream velocities and sweep angle 43.5 deg were used, resulting in edge conditions in agreement with Deyhle and Bippes's Fig. 5 for $Q_\infty = 20.5$ m/s. The traveling CF instability results in Table A5 are for the most amplified frequency $f = 180$ Hz.

Table A1 Quasiparallel results for stationary CF used in Fig. 1, based on the experimental results from Radeztsky et al.[13] (Fig. 4)

R_C	δ^*, mm	δ	$N_{\rm SCF}$	λ_z, mm
		$h_{rms} = 0.25\ \mu m$		
3.0×10^6	0.20	0.0013	9.2	10
3.3×10^6	0.18	0.0014	9.2	9
3.6×10^6	0.16	0.0016	9.0	8
		$h_{rms} = 0.51\ \mu m$		
2.6×10^6	0.23	0.0022	8.9	11
3.2×10^6	0.18	0.0028	7.9	9
3.7×10^6	0.15	0.0034	7.8	8
		$h_{rms} = 3.3\ \mu m$		
2.2×10^6	0.27	0.012	6.9	12
2.5×10^6	0.22	0.015	6.2	10
3.0×10^6	0.18	0.018	5.8	8
3.5×10^6	0.15	0.022	6.3	7

Table A2 Nonparallel results for stationary CF used in Fig. 2, based on the experimental results from Radeztsky et al.[13] (Fig. 4)

R_C	δ^*, mm	δ	$N_{\rm SCF}$	λ_z, mm
		$h_{rms} = 0.25\ \mu m$		
3.0×10^6	0.14	0.0018	9.8	10
3.3×10^6	0.13	0.0019	10.0	10
3.6×10^6	0.13	0.0019	9.9	9
		$h_{rms} = 0.51\ \mu m$		
2.6×10^6	0.16	0.0032	9.4	12
3.2×10^6	0.13	0.0039	8.8	9
3.7×10^6	0.12	0.0042	8.8	8
		$h_{rms} = 3.3\ \mu m$		
2.2×10^6	0.18	0.018	7.5	13
2.5×10^6	0.16	0.021	7.2	11
3.0×10^6	0.14	0.024	6.8	9
3.5×10^6	0.12	0.028	7.4	8

Table A3 Quasiparallel results for stationary CF used in Fig. 3 for $Tu = 0.15\%$, based on the experiments of Deyhle and Bippes[22]

R_C	δ^*, mm	δ	$N_{\rm SCF}$	λ_z, mm
1.04×10^6	0.35	0.040	9.0	11
1.15×10^6	0.32	0.0066	9.9	11
1.18×10^6	0.32	0.0055	10.0	11
1.27×10^6	0.30	0.0021	10.7	10

Table A4 Nonparallel results for stationary CF used in Fig. 4 for $Tu = 0.15\%$, based on the experiments of Deyhle and Bippes[22]

R_C	δ^*, mm	δ	$N_{\rm SCF}$	λ_z, mm
1.04×10^6	0.24	0.059	10.7	12
1.15×10^6	0.23	0.0092	11.5	11
1.18×10^6	0.23	0.0077	11.7	11
1.27×10^6	0.22	0.0029	12.4	10

Table A5 Quasiparallel and nonparallel results for traveling CF used in Fig. 5 for $Tu = 0.15\%$, based on the experiments of Deyhle and Bippes[22]

R_C	δ^*, mm	δ	$N_{\rm TCF}$	λ_z, mm
		Quasiparallel		
1.04×10^6	0.36	0.039	12.9	12
1.15×10^6	0.32	0.0066	14.2	11
1.18×10^6	0.32	0.0055	14.5	11
1.27×10^6	0.30	0.0021	15.5	11
		Nonparallel		
1.04×10^6	0.25	0.057	15.9	12
1.15×10^6	0.23	0.0092	17.2	11
1.18×10^6	0.23	0.0077	17.5	11
1.27×10^6	0.22	0.0029	18.7	11

Acknowledgments

We have benefited from discussions with W. S. Saric, H. Bippes, S. Takagi, Y. S. Kachanov, and C. L. Streett and from the helpful comments of the reviewers.

References

[1] Nield, B. N., "An Overview of the Boeing 777 High Lift Aerodynamic Design," *Aeronautical Journal*, Vol. 99, No. 989, 1995, pp. 361–371.

[2] Kusunose, K., and Cao, H. V., "Prediction of Transition Location for a 2-D Navier–Stokes Solver for Multi-Element Airfoil Configuration," AIAA Paper 94-2376, June 1994.

[3]Smith, A. M. O., and Gamberoni, A. H., "Transition, Pressure Gradient and Stability Theory," Douglas Aircraft Co., Rept. ES26388, El Segundo, CA, Aug. 1956.

[4]Van Ingen, J. L., "A Suggested Semi-Empirical Method for the Calculation of the Boundary Layer Transition Region," Univ. of Technology, Rept. UTH1-74, Delft, The Netherlands, 1956.

[5]Reed, H. L., Saric, W. S., and Arnal, D., "Linear Stability Theory Applied to Boundary Layers," *Annual Review of Fluid Mechanics*, Vol. 28, 1996, pp. 389–428.

[6]Mack, L. M., "Transition Prediction and Linear Stability Theory," *Laminar-Turbulent Transition*, CP-224, AGARD, 1977, pp. 1/1–22.

[7]Mack, L. M., "Stability of Three-Dimensional Boundary Layers on Swept Wings at Transonic Speeds," *Symposium Transsonicum III*, edited by J. Zierep and H. Oertel, Springer–Verlag, Berlin, 1989, pp. 209–223.

[8]Govindarajan, R., and Narasimha, R., "Low-Order Theories for Stability of Non-Parallel Boundary Layer Flows," *Proceedings of the Royal Society of London, Series A*, Vol. 453, No. 1967, 1997, pp. 2537–2549.

[9]Herbert, Th., "Boundary-Layer Transition—Analysis and Prediction Revisited," AIAA Paper 91-0737, Jan. 1991.

[10]Bertolotti, F. P., "Linear and Nonlinear Stability of Boundary Layers with Streamwise Varying Properties," Ph.D. Dissertation, Dept. of Mechanical Engineering, Ohio State Univ., Columbus, OH, 1991.

[11]Bertolotti, F. P., Herbert, Th., and Spalart, P. R., "Linear and Nonlinear Stability of the Blasius Boundary Layer," *Journal of Fluid Mechanics*, Vol. 242, 1992, pp. 441–474.

[12]Crouch, J. D., "Receptivity of Three-Dimensional Boundary Layers," AIAA Paper 93-0074, Jan. 1993.

[13]Radeztsky, R. H., Reibert, M. S., Saric, W. S., and Takagi, S., "Effect of Micron-Sized Roughness on Transition in Swept-Wing Flows," AIAA Paper 93-0076, Jan. 1993.

[14]Goldstein, M. E., and Hultgren, L. S., "Boundary-Layer Receptivity to Long-Wave Free-Stream Disturbances," *Annual Review of Fluid Mechanics*, Vol. 21, 1989, pp. 137–166.

[15]Saric, W. S., Reed, H. L., and Kerschen, E. J., "Leading-Edge Respectivity to Sound: Experiments, DNS, and Theory," AIAA Paper 94-2222, June 1994.

[16]Wlezien, R. W., "Measurement of Acoustic Receptivity," AIAA Paper 94-2221, June 1994.

[17]Choudhari, M., and Streett, C. L., "Theoretical Prediction of Boundary-Layer Receptivity," AIAA Paper 94-2223, June 1994.

[18]Crouch, J. D., "Theoretical Studies on the Receptivity of Boundary Layers," AIAA Paper 94-2224, June 1994.

[19]Choudhari, M., and Streett, C. L., "Boundary Layer Receptivity Phenomena in Three-Dimensional and High-Speed Boundary Layers," AIAA Paper 90-5258, Oct. 1990.

[20]Muller, B., and Bippes, H., "Experimental Study of Instability Modes in a Three-Dimensional Boundary Layer," *Proceedings of the AGARD Symposium on Fluid Dynamics of Three-Dimensional Turbulent Shear Flows and Transition*, CP-438, AGARD, 1988.

[21]Takagi, S., Saric, W. S., Radeztsky, R. H., Spencer, S. A., and Orr, D. J., "Effect of Sound and Micro-Sized Roughness on Crossflow Dominated Transition," *Bulletin of the American Physical Society*, Vol. 36, No. 10, 1991, p. 2630.

[22]Deyhle, H., and Bippes, H., "Disturbance Growth in an Unstable Three-Dimensional Boundary Layer and Its Dependence on Environmental Conditions," *Journal of Fluid Mechanics*, Vol. 316, 1996, pp. 73–113.

[23]Takagi, S., and Itoh, N., "Observation of Traveling Waves in the Three-Dimensional Boundary Layer Along a Yawed Cylinder," *Fluid Dynamics Research*, Vol. 14, No. 4, 1994, pp. 167–189.

[24]Chang, C.-L., "ECLIPSE: An Efficient Compressible Linear PSE Code for Swept-Wing Boundary Layers," High Technology, Rept. HTC-9503, Hampton, VA, April 1995.

[25]Masad, J. A., and Abdelnaser, A. S., "Transition in Flow over a Swept Cylinder: Correlation with Experimental Data," *Physics of Fluids*, Vol. 8, No. 1, 1996, pp. 285–287.

[26]Poll, D. I. A., "Some Observations of the Transition Process on the Windward Face of a Long Yawed Cylinder," *Journal of Fluid Mechanics*, Vol. 150, 1985, p. 329.

[27]Malik, M. R., and Balakumar, P., "Linear Stability of Three-Dimensional Boundary Layers: Effects of Curvature and Non-Parallelism," AIAA Paper 93-0079, Jan. 1993.

[28]Haynes, T., and Reed, H., "Numerical Simulation of Swept-Wing Vortices Using Nonlinear Parabolized Stability Equation," Society of Automotive Engineers, Paper 971479, April 1997.

[29]Ng, L. L., and Crouch, J. D., "Roughness-Induced Receptivity to Crossflow Vortices on a Swept Wing," *Physics of Fluids*, Vol. 11, No. 2, 1999, pp. 432–438.

K. Kailasanath
Associate Editor